Manipulation of Ultra-Cold Atoms Using Radio-Frequency and Microwave Radiation

Ian D. Leroux

Under the Supervision of
Dr. Joseph H. Thywissen

April 2005

Manipulation of Ultra-Cold Atoms Using Radio-Frequency and Microwave Radiation

Ian D. Leroux

Under the Supervision of
Dr. Joseph H. Thywissen

April 2005

A Thesis Submitted in Partial Fulfilment of the Requirements for the Degree of Bachelor of Applied Science

Division of Engineering Science
Faculty of Applied Science and Engineering
University of Toronto

Abstract

This document describes progress, effected as part of an ongoing effort at Toronto's Ultra-Cold Atoms Laboratory, towards the design and implementation of systems for driving transitions between hyperfine and magnetic energy levels in potassium-40 (^{40}K) and rubidium-87 (^{87}Rb) using radio-frequency and microwave electromagnetic radiation. Such forced transitions are used for evaporative cooling of trapped atoms, energy spectroscopy, and production of coherent mixtures of atoms in different quantum states. Theoretical derivations of relevant frequency and field intensity parameters are presented. The designs of the radio-frequency antenna and of one microwave signal generation section are described. Preliminary analyses of the uncompleted subsystems are presented, which may be of interest to future contributors to this project.

Acknowledgements

I would like to thank Mr. Alan Stummer for his patient help, and his insights into the real-world behaviour of electronic components. Drs. Seth Aubin and Stefan Myrskog graciously bore my interference with their apparatus, and were cheerfully helpful when that interference produced undesirable side-effects. Finally, I am grateful to Dr. Joseph Thywissen for inviting me into his research group, introducing me to the fascinating world of atomic physics, guiding me along the sometimes tortuous path to this document and providing me with a good deal of wise counsel, much of it well outside the scope of this project.

Contents

Contents iii

List of Symbols iv

List of Figures vi

List of Tables vii

1 Introduction 1

2 Theory of Magnetic Levels and Transitions 4
- 2.1 The Magnetic Dipole Moment Operator 4
- 2.2 Level Splittings 6
- 2.3 Frequency Selection 7
- 2.4 Transition Matrix Elements 9
- 2.5 Transition Probabilities and Field Amplitudes 13

3 Design and Implementation 15
- 3.1 Radio-Frequency Antenna and Coupler Circuit 16
- 3.2 Microwave Signal Generation for ^{40}K 19
- 3.3 Comments on Microwave Signal Generation for ^{87}Rb 20
- 3.4 Comments on Microwave Antennae 21

4 Conclusion 23

Bibliography 24

A Power Supply for the ^{40}K Microwave System 26

List of Symbols

a	arbitrary scalar
$\|a\rangle$	arbitrary basis ket
B	magnetic flux density
B_{osc}	oscillating magnetic field magnitude
B_{static}	static magnetic field magnitude
b	arbitrary scalar
$\|b\rangle$	arbitrary basis ket
c	speed of light in free space
E	energy
e	elementary charge
$\boldsymbol{e_x}$	unit vector along the x axis
$\boldsymbol{e_z}$	unit vector along the z axis
F	atomic angular momentum quantum number
$\widehat{\boldsymbol{F}}$	atomic angular momentum operator
$\widehat{F}_z$	z-axis atomic angular momentum operator
g	Landé g-factor (in general)
g_F	Landé g-factor of the atom
$\hbar$	quantum of angular momentum
$\widehat{H}$	Hamiltonian operator
$\widehat{H}^0$	time-independent Hamiltonian
$\widehat{H}_{eff}$	effective Hamiltonian
I	nuclear spin quantum number or electric current, according to context
i	imaginary number $\sqrt{-1}$
$\widehat{\boldsymbol{I}}$	nuclear spin operator
$\widehat{\boldsymbol{J}}$	angular momentum operator
k_B	Boltzmann's constant
$\widehat{\boldsymbol{L}}$	orbital angular momentum operator
m	mass
m_e	mass of the electron
m_F	z-axis atomic angular momentum quantum number
m_I	z-axis nuclear spin quantum number
m_p	mass of the proton
m_S	z-axis electron spin quantum number
P	probability

q	electric charge
r	radial distance
S	electron spin quantum number
$\widehat{\boldsymbol{S}}$	electron spin operator
$\widehat{S}_x$	x-axis electron spin operator
$\widehat{S}_z$	z-axis electron spin operator
T	temperature
U	magnetic trapping potential
V	perturbing potential amplitude
v_T	thermal velocity of the atom
$\widehat{V}$	perturbing potential operator
γ	gyromagnetic ratio
η	impedance of free space
θ	polar angle
λ	wavelength
$\widehat{\boldsymbol{\mu}}$	magnetic moment operator
μ_B	Bohr magneton ($e\hbar/2m_e c$)
μ_N	nuclear magneton ($e\hbar/2m_p c$)
μ_0	magnetic permeability of free space
π	ratio of a circle's circumference to its diameter
ψ	quantum state vector
ω	angular frequency
ω_{HF}	hyperfine splitting, in angular frequency units
ω_0	level separation of an arbitrary time-independent two-level system, in angular frequency units

List of Figures

2.1 Schematic of relevant energy levels in ^{40}K 8

3.1 Layout of wires on the chip 16
3.2 Radio-frequency coupler circuit 17
3.3 Schematic of radio-frequency signal generation, amplification, and transmission system 18
3.4 Schematic of ^{40}K microwave signal generation system 20

A.1 Schematic of ^{40}K microwave generator power supply 27

List of Tables

2.1 Selected transition amplitudes for ^{40}K and ^{87}Rb, expressed as multiples of $\mu_B B_{osc}$ 13

Chapter 1

Introduction

The Heisenberg uncertainty principle dictates that, if a group of particles is sufficiently cold and sufficiently dense, the wavefunctions of its constituent particles will begin to overlap in space. This peculiar state of affairs, in which the particles cease to be spatially distinct objects and partially merge into single cloud, is known as quantum degeneracy. Interestingly, although their theoretical treatment can be traced back to the work of Bose and Einstein in the mid-1920s, the technical difficulties of cooling atoms sufficiently have prevented the experimental study of dilute quantum-degenerate clouds of atoms until comparatively recently. A Bose-Einstein Condensate — a quantum-degenerate cloud of bosons — was first created in 1995[1][2][3], and a quantum-degenerate Fermi gas was achieved in 1999[4][5][6].

The study of quantum-degenerate atomic gases has attracted considerable attention since then for a number of reasons. First, the length scales for quantum phenomena in such systems are within reach of standard optical measurement tools; one can directly take pictures of quantum effects. Second, the systems are amenable to theoretical treatment; the density of atoms and the complexity of their behaviour are both low enough that tractable analytic models give good results. The combination of direct observation and theoretical analysis of non-classical behaviour allows for a variety of good tests of our understanding of quantum mechanics. Third, the physics of quantum degeneracy is thought to be involved in a number of fascinating, ill-understood, and potentially useful phenomena such as superconductivity and superfluidity. Finally, by offering macroscopic and manipulable objects with quantum behaviour, quantum-degenerate gas systems may be useful to the fledgling field of quantum information processing.

The Ultra-Cold Atoms Laboratory at the University of Toronto, operating since early in 2003, is taking an active part in this broad research effort. Its activities focus on the development of new techniques for the creation of quantum-degenerate mixtures of fermionic

potassium-40 (^{40}K) and bosonic rubidium-87 (^{87}Rb) confined in "chip traps": magnetic potential wells created with microfabricated wires. A detailed description of the current experimental apparatus and its capabilities was recently given in [7].

In order to carry out its experimental programme successfully, the Ultra-Cold Atoms Laboratory requires the ability to subject the trapped atoms to various forms of electro-magnetic radiation. This radiation, or more specifically the associated oscillating magnetic field, serves to drive transitions between atomic states of different energies. The ability to induce such transitions has several uses: it allows a cooling technique known as forced evaporative cooling, it can be used to determine the energy distribution of atoms in the trapped cloud, and it can be used to create coherent mixtures of different atomic states.

The technique of evaporative cooling is a crucial step in the process of bringing an atomic cloud to quantum degeneracy[8]. In essence, it involves the selective ejection of the hottest atoms in the atomic cloud. As these carry away more than their share of the cloud's energy, the average energy of the remaining atoms — and hence the temperature — decreases. If the atoms of the cloud collide often enough, they will return to a normal thermal energy distribution with a high-energy tail, which can in turn be ejected from the trap, continuing the process. Under the right conditions, as the cut-off energy for ejection from the trap is swept downwards, a portion of the atoms will be cooled into the lowest available energy states, leading to quantum degeneracy. The most common method of ejecting the hot atoms is to transfer them to an atomic state that is not confined by the magnetic trap (c.f. Section 2.2).

The same experimental tools can be used to determine the energy distribution in a cloud of atoms. Using optical absorption or fluorescence it is possible to measure, at any given point in time, the number of atoms in the cloud. Making such a measurement, rapidly transferring all atoms above a certain energy to untrapped states without giving time for them to re-thermalise, and measuring the surviving population gives a measure of the proportion of atoms that have less than the selected cut-off energy. Multiple iterations of this procedure can generate a complete profile of the cloud's energy distribution[9].

The ability to transfer rapidly a portion of a cloud of atoms to a different state is also intrinsically interesting. If the initial cloud was in a well-understood quantum state, this transfer allows the creation of a quantum state with two interrelated components, one for each part of the separated mixture. Such two-dimensional quantum states have a much richer phenomenology than their one-dimensional counterparts, opening interesting new avenues for exploration.

The project described herein is the design and construction of the systems necessary to transfer atoms between energy states using electro-magnetic radiation. Three systems

are required: one to operate in the radio-frequency range of $2\pi \times (0.5 - 30)$ MHz[1] for evaporative cooling of both ^{40}K and ^{87}Rb, and two to operate in the microwave region at $2\pi \times (1.186 - 1.386)$ GHz and $2\pi \times (6.751 - 6.919)$ GHz for more precise control of ^{40}K and ^{87}Rb respectively. In each of these systems an appropriate signal must be generated, amplified, and transmitted by means of some appropriate antenna.

The remainder of this document is divided as follows. Chapter 2 examines the problem from a theoretical standpoint, discussing the atomic energy levels involved, the spacing between them, and the effect of an oscillating magnetic field in transferring atoms from one to another. This theoretical treatment serves to establish the performance requirements for the systems to be constructed. Chapter 3 takes a more pragmatic stance, presenting some additional real-world constraints and describing those systems that have been designed and implemented. Chapter 4 presents a brief conclusion and Appendix A describes the design of the power supply for the ^{40}K microwave system.

[1] Radian or angular frequency will be used throughout, for consistency. To obtain conventional frequency values, ignore the prefactor of 2π.

Chapter 2

Theory of Magnetic Levels and Transitions

The electromagnetic wave to which the atoms will be subjected can effectively be described by two parameters: amplitude and frequency. The physical characteristics of the level change process impose certain restrictions on these parameters, which in turn set the basic performance requirements of the radio-frequency and microwave systems to be designed.

The physical phenomena in play are briefly described. The first of these is the magnetic dipole moment of the atom, which encapsulates as much of its behaviour as is needed to understand this project. Next come the separations of the various energy levels, which set the frequency requirements. Finally, the oscillating magnetic field introduces a coupling between energy levels, and determines the necessary field amplitudes to make that coupling useful.

2.1 The Magnetic Dipole Moment Operator

The magnetic dipole moment of the atom can have three sources: the orbital motion of the electrons, the intrinsic angular momentum or spin of the electrons, and the spin of the nucleus. Each of these makes a contribution of the form

$$\widehat{\boldsymbol{\mu}} = \gamma \widehat{\boldsymbol{J}} \tag{2.1}$$

where $\widehat{\boldsymbol{J}}$ is the relevant angular momentum operator ($\widehat{\boldsymbol{L}}$, $\widehat{\boldsymbol{S}}$ or $\widehat{\boldsymbol{I}}$ respectively).

The gyromagnetic ratio γ is -μ_B for orbital electronic angular momentum, $-2\mu_B$ for electronic spin[1], $-1.298100\,\mu_N$ for the ^{40}K nucleus and $+2.75124\,\mu_N$ for ^{87}Rb nucleus[11,

[1]The g-2 correction for the electron is $\approx 2 \times 10^{-3}$ [10, p.390], and will be ignored in this treatment.

p9-94]. Here μ_B is the Bohr magneton and μ_N is the nuclear magneton. Since the latter is smaller by a factor of $m_e/m_p \approx 5 \times 10^{-4}$ and since the nuclear spin is never more than eight times the electron spin for the atoms and states under consideration, the nuclear spin contribution will be smaller by a factor of at least 167 compared to the electronic spin term and will be neglected hereafter.

The fact that we will only be treating alkali atoms in the ground state leads to further simplifications. First, the electrons have no orbital angular momentum in the ground state, so that only the electronic spin term remains. Second, alkali atoms are precisely those that have a single valence electron. According to the Aufbau principle, in the ground state all other electrons will be bound in lower-energy states in pairs of opposite spin. The total spin contribution of each of these pairs is zero, so we are left with only the contribution from the spin of the valence electron, which is

$$\widehat{\boldsymbol{\mu}} = -\frac{2\mu_B}{\hbar}\widehat{\boldsymbol{S}} \tag{2.2}$$

Since $\widehat{\boldsymbol{\mu}}$ is now simply a scalar multiple of an angular momentum operator, it is a vector operator in the sense of the Wigner-Eckart Theorem. This implies that, within a subspace of fixed total atomic angular momentum[2], the magnetic dipole operator ($\widehat{\boldsymbol{\mu}}$) is proportional to the total atomic angular momentum operator ($\widehat{\boldsymbol{F}}$). The Projection Theorem[12, p1054] and the fact that $\widehat{\boldsymbol{F}} = \widehat{\boldsymbol{I}} + \widehat{\boldsymbol{S}}$ in the absence of orbital angular momentum allow a straightforward computation of the proportionality constant

$$\begin{aligned}
\widehat{\boldsymbol{\mu}} &= \frac{\left\langle \widehat{\boldsymbol{F}} \cdot \widehat{\boldsymbol{\mu}} \right\rangle}{F(F+1)\hbar^2}\widehat{\boldsymbol{F}} && (2.3)\\
&= -\frac{2\mu_B \left\langle \widehat{\boldsymbol{F}} \cdot \widehat{\boldsymbol{S}} \right\rangle}{F(F+1)\hbar^3}\widehat{\boldsymbol{F}} && (2.4)\\
&= -\frac{2\mu_B \left\langle (\widehat{\boldsymbol{I}} + \widehat{\boldsymbol{S}}) \cdot \widehat{\boldsymbol{S}} \right\rangle}{F(F+1)\hbar^3}\widehat{\boldsymbol{F}} && (2.5)\\
&= -\frac{2\mu_B \left\langle \widehat{\boldsymbol{I}} \cdot \widehat{\boldsymbol{S}} + \widehat{\boldsymbol{S}}^2 \right\rangle}{F(F+1)\hbar^3}\widehat{\boldsymbol{F}} && (2.6)\\
&= -\frac{2\mu_B \left\langle \frac{1}{2}(\widehat{\boldsymbol{F}}^2 - \widehat{\boldsymbol{I}}^2 - \widehat{\boldsymbol{S}}^2) + \widehat{\boldsymbol{S}}^2 \right\rangle}{F(F+1)\hbar^3}\widehat{\boldsymbol{F}} && (2.7)\\
&= -\frac{\mu_B \left\langle \widehat{\boldsymbol{F}}^2 - \widehat{\boldsymbol{I}}^2 + \widehat{\boldsymbol{S}}^2 \right\rangle}{F(F+1)\hbar^3}\widehat{\boldsymbol{F}} && (2.8)\\
\widehat{\boldsymbol{\mu}} &= -\frac{\mu_B(F(F+1) - I(I+1) + S(S+1))}{F(F+1)\hbar}\widehat{\boldsymbol{F}} && (2.9)
\end{aligned}$$

[2] That is, within a single hyperfine level.

This can be more conveniently expressed as

$$\widehat{\boldsymbol{\mu}} = -g_F \frac{\mu_B}{\hbar} \widehat{\boldsymbol{F}} \tag{2.10}$$

$$g_F = \frac{F(F+1) - I(I+1) + S(S+1)}{F(F+1)} \tag{2.11}$$

Since the electron has spin $\frac{1}{2}$ and F varies by integer steps in the range $|I - S| \leq F \leq I + S$, we must have $F = I \pm \frac{1}{2}$. The corresponding values of g_F are

$$g_F = \frac{(I \pm \frac{1}{2})(I \pm \frac{1}{2} + 1) - I(I+1) + \frac{1}{2}(\frac{1}{2} + 1)}{(I \pm \frac{1}{2})(I \pm \frac{1}{2} + 1)} \tag{2.12}$$

$$= \frac{I^2 \pm \frac{1}{2}I + I \pm \frac{1}{2}I + \frac{1}{4} \pm \frac{1}{2} - I^2 - I + \frac{3}{4}}{I^2 \pm \frac{1}{2}I + I \pm \frac{1}{2}I + \frac{1}{4} \pm \frac{1}{2}} \tag{2.13}$$

$$= \frac{\pm I \pm \frac{1}{2} + 1}{(I + \frac{1}{2} \pm 1)} \frac{1}{(I + \frac{1}{2})} \tag{2.14}$$

$$g_F = \pm \frac{2}{2I + 1} \tag{2.15}$$

with the + case corresponding to $F = I + \frac{1}{2}$. For ^{40}K, $I = 4$ so that $F = \frac{9}{2}$ and $g_F = \pm\frac{2}{9}$ while for ^{87}Rb, $I = \frac{3}{2}$, $F = 2$ and $g_F = \pm\frac{1}{2}$

2.2 Level Splittings

There are two level splittings of interest in this problem, one fixed and one controllable. The fixed one is the hyperfine split, due to the dipole-dipole interaction between the nuclear magnetic moment and the electron spin magnetic moment. In one F-level the two magnetic moments are parallel and in the other they are anti-parallel. The difference in interaction energies breaks the degeneracy between them. The energy separation is a fixed atomic property, empirically determined. For ^{40}K the $F = 7/2$ level is $\hbar \times 2\pi \times 1.286$ GHz above the $F = 9/2$ level while for ^{87}Rb the $F = 2$ level is $\hbar \times 2\pi \times 6.835$ GHz above the $F = 1$ level.

The second level separation to be considered is the Zeeman shift, whose size can be computed as follows. Consider a single atom in the ground state in either of the two hyperfine levels, and add a static magnetic field $B_{static}\boldsymbol{e_z}$ along the x-axis[3]. The corresponding

[3]Without loss of generality, since the system was initially isotropic.

additional term in the Hamiltonian is

$$\widehat{V} = -\widehat{\boldsymbol{\mu}} \cdot B_{static} \boldsymbol{e_z} \tag{2.16}$$

Perturbation theory gives the first-order energy shift for each state as $\left\langle \widehat{V} \right\rangle$, which is readily computed from the special-case formula 2.10 as follows

$$\begin{aligned} \langle Fm_F | \widehat{V} | Fm_F \rangle &= -\langle Fm_F | \widehat{\boldsymbol{\mu}} \cdot B_{static} \boldsymbol{e_z} | Fm_F \rangle & (2.17) \\ &= g_F \frac{\mu_B}{\hbar} \langle Fm_F | \widehat{\boldsymbol{F}} \cdot B_{static} \boldsymbol{e_z} | Fm_F \rangle & (2.18) \\ &= g_F \frac{\mu_B}{\hbar} B_{static} \langle Fm_F | \widehat{F}_z | Fm_F \rangle & (2.19) \\ U &= g_F m_F \mu_B B_{static} & (2.20) \end{aligned}$$

The different m_F states are shifted in energy by an amount directly proportional to the magnitude of the external magnetic field. A static field configuration with a local minimum in field strength thus defines a potential well for atomic states whose $g_F m_F$ product is positive: a magnetic trap.

An atom can be ejected from the trap simply by transferring it to a state whose $g_F m_F$ product is negative, so that the potential becomes repulsive. Note that the hotter or more energetic an atom, the further up the sides of the potential well it will travel as it orbits in the trap, and the stronger the magnetic fields it will experience. Since the energy shifts of the m_F states are proportional to the field strength, the hotter atoms will, at times, exhibit larger energy shifts than those of colder atoms. By tuning the frequency of an oscillating field so that it is resonant with a transition only when the levels have been sufficiently displaced, atoms at or above a certain temperature may be selectively manipulated. It is this ability to select only those atoms with a certain minimum energy that allows for evaporative cooling and energy spectroscopy.

2.3 Frequency Selection

The resonant frequency for a transition is set by

$$\frac{\Delta U}{\hbar} = \frac{(g'_F m'_F - g_F m_F)\mu_B B_{static}}{\hbar} + [\omega_{HF}] \tag{2.21}$$

where ω_{HF} is the hyperfine splitting which must be added in for transitions that change F level. For $\Delta m_F = \pm 1$ transitions within a single F level, the $(g'_F m'_F - g_F m_F)$ factor is $\pm 2/9$ for ^{40}K, giving $2\pi \times 3.11$ GHz/T; and $\pm 1/2$ for ^{87}Rb, giving $2\pi \times 7.00$ GHz/T. The

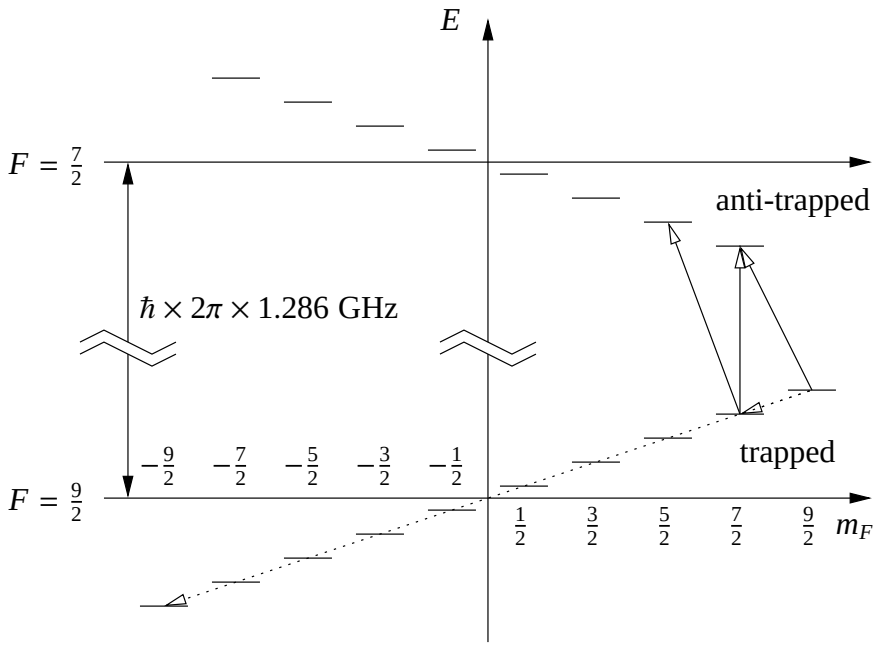

Figure 2.1: Schematic of relevant energy levels of ^{40}K (not to scale)

Open-headed arrows indicate interesting transitions from trapped to untrapped states, with solid lines for microwave transitions and dashed lines for radio-frequency transitions. For the energy separation of the m_F steps, see Section 2.3. Note that in the radio-frequency case, although the atom is transferred to the $m_F = -\frac{9}{2}$ state, the radio-frequency coupling is done by steps of $\Delta m_F = -1$, since that is the only allowed transition (see Section 2.4).

maximum field in the trap is 4 mT, so that the highest frequency required of the radio-frequency system which deals with transitions within the same F level is $2\pi \times 28.0$ MHz. The minimum field is 0.1 mT, leading to a theoretical minimum frequency requirement of $2\pi \times 311$ kHz. However, a signal at this frequency would remove all atoms from the trap. This is not only unnecessary but undesirable; in practise it is sufficient to reach $2\pi \times 500$ kHz[13]. Finally, the trap field is only stable to within 1 μT, so that the smallest frequency difference of any experimental significance is $2\pi \times 3$ kHz. This sets the criterion for frequency precision; in order to control the energy of the affected atoms as well as possible, the frequencies must be accurate to within $2\pi \times 3$ kHz[4].

For transitions between F levels, the $(g'_F m'_F - g_F m_F)$ factor can range from $-16/9$ to $16/9$ in ^{40}K or -3 to 3 in ^{87}Rb. Not all these transitions are needed for evaporative cooling, but the remaining ones are potentially useful either for creation of coherent mixtures or for accessing certain inter-atomic bound states (Feschbach resonances) and are included for completeness. The frequency ranges, shifted up by the respective hyperfine splitting, are

[4] At least at the end of a frequency sweep.

therefore $2\pi \times (1.186 - 1.386)$ GHz for ^{40}K and $2\pi \times (6.751 - 6.919)$ GHz for ^{87}Rb. The precision requirements are $2\pi \times 3$ kHz for ^{40}K and $2\pi \times 7$ kHz for ^{87}Rb.

2.4 Transition Matrix Elements

We now consider the problem of transferring atoms between states using a resonant perturbation. Consider two levels $|a\rangle$ and $|b\rangle$ of a system, separated in energy by $\hbar\omega_0$. If we ignore all other energy levels in the system[5], the time-independent Schrödinger equation may be written as

$$\widehat{H}^0\psi = i\hbar\dot{\psi} \tag{2.22}$$

with

$$\psi = \begin{pmatrix} ae^{-i\frac{\omega_0}{2}t} \\ be^{i\frac{\omega_0}{2}t} \end{pmatrix} \quad \widehat{H}^0 = \begin{pmatrix} \frac{\hbar\omega_0}{2} & 0 \\ 0 & -\frac{\hbar\omega_0}{2} \end{pmatrix} \tag{2.23}$$

where $ae^{-i\frac{\omega_0}{2}t}$ and $be^{i\frac{\omega_0}{2}t}$ are the amplitudes of the two basis kets $|a\rangle$ and $|b\rangle$ in the combined state and the point of zero energy is chosen halfway between the two energy levels. Now add an oscillating perturbation operator

$$\widehat{V}_{(t)} = \cos\omega t \begin{pmatrix} 0 & V \\ V^\star & 0 \end{pmatrix} \tag{2.24}$$

which couples these two levels. The Schrödinger equation becomes

$$\begin{pmatrix} \frac{\hbar\omega_0}{2} & \frac{V}{2}(e^{i\omega t} + e^{-i\omega t}) \\ \frac{V^\star}{2}(e^{i\omega t} + e^{-i\omega t}) & -\frac{\hbar\omega_0}{2} \end{pmatrix} \begin{pmatrix} ae^{-i\frac{\omega_0}{2}t} \\ be^{i\frac{\omega_0}{2}t} \end{pmatrix} = i\hbar\frac{\partial}{\partial t}\begin{pmatrix} ae^{-i\frac{\omega_0}{2}t} \\ be^{i\frac{\omega_0}{2}t} \end{pmatrix} \tag{2.25}$$

Carrying out the time derivative and simplifying gives

$$\begin{pmatrix} \frac{V}{2}(e^{i(\omega_0+\omega)t} + e^{i(\omega_0-\omega)t})b \\ \frac{V^\star}{2}(e^{-i(\omega_0+\omega)t} + e^{-i(\omega_0-\omega)t})a \end{pmatrix} = i\hbar\begin{pmatrix} \dot{a} \\ \dot{b} \end{pmatrix} \tag{2.26}$$

Assuming the perturbation is resonant ($\omega = \omega_0$) and neglecting the rapidly oscillating off-resonant $e^{i(\omega+\omega_0)t}$ contributions — i.e. making the rotating wave approximation[14] — gives

$$\widehat{H}_{eff}\begin{pmatrix} a \\ b \end{pmatrix} = i\hbar\begin{pmatrix} \dot{a} \\ \dot{b} \end{pmatrix} \tag{2.27}$$

[5] An approximation usually justified *a posteriori* by stipulating that other level transitions are not resonant with the perturbing field's oscillation frequency.

where

$$\widehat{H}_{eff} = \begin{pmatrix} 0 & \frac{V}{2} \\ \frac{V^\star}{2} & 0 \end{pmatrix} \tag{2.28}$$

This has the form of the time-independent Schrödinger equation with a static effective coupling $\frac{V}{2}$.

The specific perturbation of interest is an oscillating magnetic field

$$B_{osc}(\boldsymbol{e_z}\cos\theta + \boldsymbol{e_x}\sin\theta)\cos\omega t \tag{2.29}$$

perpendicular to the static field and chosen here to be in the $x-z$ plane[6]. The corresponding time-dependent coupling matrix element is

$$\begin{aligned}
\widehat{V}\cos\omega t &= -\langle F' m'_F \big| \widehat{\boldsymbol{\mu}} \cdot B_{osc}(\boldsymbol{e_z}\cos\theta + \boldsymbol{e_x}\sin\theta)\cos\omega t \, |F m_F\rangle && (2.30)\\
&= \frac{2\mu_B}{\hbar} B_{osc}\cos\omega t \, \langle F' m'_F \big| \widehat{\boldsymbol{S}} \cdot (\boldsymbol{e_z}\cos\theta + \boldsymbol{e_x}\sin\theta) \, |F m_F\rangle && (2.31)\\
&= \frac{2\mu_B}{\hbar} B_{osc}\cos\omega t \, \langle F' m'_F \big| \left(\widehat{S}_z\cos\theta + \widehat{S}_x\sin\theta\right) |F m_F\rangle && (2.32)
\end{aligned}$$

Assuming the diagonal elements of the coupling matrix to be negligibly small in comparison to the diagonal elements of the unperturbed Hamiltonian, this has the same form as the $\widehat{V}$ discussed above. The effective static coupling amplitude is therefore

$$\frac{V}{2} = \frac{\mu_B}{\hbar} B_{osc} \, \langle F' m'_F \big| \left(\widehat{S}_z\cos\theta + \widehat{S}_x\sin\theta\right) |F m_F\rangle \tag{2.33}$$

The $\cos\theta$ and $\sin\theta$ factors are suppressed hereafter both for convenience and because the orientation of the static trapping field, which serves to define the z-axis, varies throughout the trap, such that every possible value of the angle θ between trapping field and oscillating field occurs at some point.

We now treat the $\widehat{S}_x$ and $\widehat{S}_z$ terms separately. The $\widehat{S}_x$ term becomes

$$\frac{\mu_B}{\hbar} B_{osc} \sum_{\substack{m'_I, m'_S \\ m_I, m_S}} \langle F' m'_F \big| \, I m'_I, S m'_S \rangle \, \langle I m'_I, S m'_S \big| \widehat{S}_x \, | I m_I, S m_S \rangle \, \langle I m_I, S m_S | \, F m_F \rangle \tag{2.34}$$

where we have introduced a resolution of unity on either side of the $\widehat{S}_x$ operator. Now $\widehat{S}_x$ acts as the identity operator ($\delta_{m'_I, m_I}$) over the nuclear spin subspace. Explicitly evaluating it

[6] Still without loss of generality, as the system was previously cylindrically symmetric about the z-axis.

in the electron spin space, knowing that $S = \frac{1}{2}$, gives

$$\begin{aligned} & \frac{\mu_B}{\hbar} B_{osc} \sum_{\substack{m'_I, m'_S \\ m_I, m_S}} \left\langle F' m'_F \right| I m'_I, \tfrac{1}{2} m'_S \left\rangle \delta_{m'_I, m_I \frac{\hbar}{2}} \right. \\ & \left. \times \left(\delta_{m'_S, -\frac{1}{2}} \delta_{m_S, +\frac{1}{2}} + \delta_{m'_S, +\frac{1}{2}} \delta_{m_S, -\frac{1}{2}} \right) \left\langle I m_I, \tfrac{1}{2} m_S \right| F m_F \right\rangle \end{aligned} \tag{2.35}$$

$$\begin{aligned} = \; & \frac{1}{2} \mu_B B_{osc} \sum_{m_I} \left(\left\langle F' m'_F \right| I m_I, \tfrac{1}{2} \; -\tfrac{1}{2} \right\rangle \left\langle I m_I, \tfrac{1}{2}\tfrac{1}{2} \right| F m_F \right\rangle \\ & \left. + \left\langle F' m'_F \right| I m_I, \tfrac{1}{2}\tfrac{1}{2} \right\rangle \left\langle I m_I, \tfrac{1}{2} \; -\tfrac{1}{2} \right| F m_F \right\rangle \Big) \end{aligned} \tag{2.36}$$

Each factor in the two terms of the summand is a Clebsch-Gordan coefficient, which must vanish unless the z-components of angular momentum are consistent, that is unless $m_F = m_I + m_S$. Imposing this constraint and carrying out the summation gives

$$\begin{aligned} & \frac{1}{2} \mu_B B_{osc} \left(\delta_{m'_F, m_F - 1} \left\langle F' m'_F \right| I \, m'_F + \tfrac{1}{2}, \tfrac{1}{2} \; -\tfrac{1}{2} \right\rangle \left\langle I \, m_F - \tfrac{1}{2}, \tfrac{1}{2}\tfrac{1}{2} \right| F m_F \right\rangle \\ & + \delta_{m'_F, m_F + 1} \left\langle F' m'_F \right| I \, m'_F - \tfrac{1}{2}, \tfrac{1}{2}\tfrac{1}{2} \right\rangle \left\langle I \, m_F + \tfrac{1}{2}, \tfrac{1}{2} \; -\tfrac{1}{2} \right| F m_F \right\rangle \Big) \end{aligned} \tag{2.37}$$

$$\begin{aligned} = \; & \frac{1}{2} \mu_B B_{osc} \left(\begin{array}{l} \delta_{F', F, I \pm \frac{1}{2}} \left(\pm \delta_{m'_F, m_F - 1} \sqrt{\frac{I \mp m'_F + \frac{1}{2}}{2I+1}} \sqrt{\frac{I \pm m_F + \frac{1}{2}}{2I+1}} \right. \\ \qquad \left. \pm \delta_{m'_F, m_F + 1} \sqrt{\frac{I \pm m'_F + \frac{1}{2}}{2I+1}} \sqrt{\frac{I \mp m_F + \frac{1}{2}}{2I+1}} \right) \\ + \delta_{F', I \pm \frac{1}{2}} \delta_{F, I \mp \frac{1}{2}} \left(\mp \delta_{m'_F, m_F - 1} \sqrt{\frac{I \mp m'_F + \frac{1}{2}}{2I+1}} \sqrt{\frac{I \mp m_F + \frac{1}{2}}{2I+1}} \right. \\ \qquad \left. \pm \delta_{m'_F, m_F + 1} \sqrt{\frac{I \pm m'_F + \frac{1}{2}}{2I+1}} \sqrt{\frac{I \pm m_F + \frac{1}{2}}{2I+1}} \right) \end{array} \right) \end{aligned} \tag{2.38}$$

This expression describes two types of transition. For a transition $m_F \rightarrow m_F \pm 1$ within the same F level, it reduces to

$$\frac{1}{4} g_F \mu_B B_{osc} \sqrt{F(F+1) - m_F(m_F \pm 1)} \tag{2.39}$$

For a transition connecting m_F in the $F = I + \frac{1}{2}$ hyperfine level to or from $m_F \pm 1$ in the $F = I - \frac{1}{2}$ hyperfine level it gives

$$\mp \frac{1}{2} \frac{\mu_B B_{osc}}{2I+1} \sqrt{(I \mp m_F)^2 - \frac{1}{4}} \tag{2.40}$$

The treatment of the $\widehat{S}_z$ term is similar to that just completed for the $\widehat{S}_x$ term, viz.

$$\frac{\mu_B}{\hbar}B_{osc}\sum_{\substack{m_I',m_S'\\ m_I,m_S}}\langle F'm_F'|\, Im_I', S\,m_S'\rangle\,\langle Im_I', S\,m_S'|\,\widehat{S}_z\,|Im_I, S\,m_S\rangle\,\langle Im_I, S\,m_S|\, Fm_F\rangle \tag{2.41}$$

$$= \frac{\mu_B}{\hbar}B_{osc}\sum_{\substack{m_I',m_S'\\ m_I,m_S}} \left\langle F'm_F'\right|\, Im_I', \tfrac{1}{2}m_S'\Big\rangle\,\delta_{m_I',m_I}\tfrac{\hbar}{2} \times\left(\delta_{m_S',m_S,+\frac{1}{2}}-\delta_{m_S',m_S,-\frac{1}{2}}\right)\Big\langle Im_I, \tfrac{1}{2}m_S\Big|\, Fm_F\Big\rangle \tag{2.42}$$

$$= \frac{1}{2}\mu_B B_{osc}\sum_{m_I}\left(\Big\langle F'm_F'\Big|\, Im_I, \tfrac{1}{2}\tfrac{1}{2}\Big\rangle\Big\langle Im_I, \tfrac{1}{2}\tfrac{1}{2}\Big|\, Fm_F\Big\rangle - \Big\langle F'm_F'\Big|\, Im_I, \tfrac{1}{2}\ -\tfrac{1}{2}\Big\rangle\Big\langle Im_I, \tfrac{1}{2}\ -\tfrac{1}{2}\Big|\, Fm_F\Big\rangle\right) \tag{2.43}$$

$$= \frac{1}{2}\mu_B B_{osc}\delta_{m_F',m_F}\left(\Big\langle F'm_F'\Big|\, I\,m_F'-\tfrac{1}{2}, \tfrac{1}{2}\tfrac{1}{2}\Big\rangle\Big\langle I\,m_F-\tfrac{1}{2}, \tfrac{1}{2}\tfrac{1}{2}\Big|\, Fm_F\Big\rangle - \Big\langle F'm_F'\Big|\, I\,m_F'+\tfrac{1}{2}, \tfrac{1}{2}\ -\tfrac{1}{2}\Big\rangle\Big\langle I\,m_F+\tfrac{1}{2}, \tfrac{1}{2}\ -\tfrac{1}{2}\Big|\, Fm_F\Big\rangle\right) \tag{2.44}$$

The only transition that this expression allows is a change of F while preserving m_F, with amplitude

$$-\frac{\mu_B B_{osc}}{2I+1}\sqrt{I(I+1)-m_F^2+\frac{1}{4}} \tag{2.45}$$

Note that the transitions generated by the axial (z) portion of the perturbation operator always change m_F by 1, whereas those generated by the radial (x) portion of the perturbation operator always leave m_F unchanged. Thus, only one of the two contributes to any given transition.

We are now better placed to understand the reasons for using F-changing transitions at all, despite the technical difficulties of operating in the GHz frequency range. Since the m_F states within a single F level are evenly spaced and since the perturbation operator only couples adjacent m_F sublevels, transferring atoms between them using radio-frequency transitions requires simultaneously coupling together all the m_F sublevels in each hyperfine level. Using ^{40}K as an example, this makes it practically impossible in certain cases to transfer atoms from the $m_F = \frac{9}{2}$ to $-\frac{9}{2}$ states without also transferring some to $\frac{7}{2}$, $\frac{5}{2}$ and so forth, thus creating an uncontrolled and undesirable mixture of states. The use of hyperfine transitions corrects this shortcoming. Because of the different values of the $(g_F'm_F' - g_F m_F)$ factor (see Equation 2.21), the energy spacing between states of different F varies from pair to pair, so that transitions that change F couple only the desired levels. This additional control avoids the contamination problem described above, and permits selective addressing of individual m_F sublevels.

Species	Coupled States (F,m_F)		Amplitude ($\times\mu_B B_{osc}$)
^{40}K	$\frac{9}{2}, \frac{9}{2}$	$\frac{7}{2}, \frac{7}{2}$	$\sqrt{\frac{2}{9}} \approx 0.471$
^{40}K	$\frac{9}{2}, \frac{7}{2}$	$\frac{7}{2}, \frac{5}{2}$	$\frac{\sqrt{14}}{9} \approx 0.416$
^{40}K	$\frac{9}{2}, \frac{7}{2}$	$\frac{7}{2}, \frac{7}{2}$	$-\frac{\sqrt{8}}{9} \approx -0.314$
^{40}K	$\frac{9}{2}, \frac{9}{2}$	$\frac{9}{2}, \frac{7}{2}$	$\frac{1}{6} \approx 0.167$
^{40}K	$\frac{9}{2}, \frac{7}{2}$	$\frac{9}{2}, \frac{5}{2}$	$\frac{2}{9} \approx 0.222$
^{40}K	$\frac{9}{2}, \frac{5}{2}$	$\frac{9}{2}, \frac{3}{2}$	$\frac{\sqrt{7}}{6\sqrt{4}} \approx 0.255$
^{40}K	$\frac{9}{2}, \frac{3}{2}$	$\frac{9}{2}, \frac{1}{2}$	$\frac{\sqrt{2}}{3\sqrt{3}} \approx 0.272$
^{40}K	$\frac{9}{2}, \frac{1}{2}$	$\frac{9}{2}, -\frac{1}{2}$	$\frac{5}{18} \approx 0.278$
... and symmetrically for $-m_F \rightarrow -m_F - 1$			
^{87}Rb	2,2	1,1	$\frac{\sqrt{3}}{4} \approx 0.433$
^{87}Rb	2,1	1,0	$\frac{\sqrt{3}}{4\sqrt{2}} \approx 0.306$
^{87}Rb	2,1	1,1	$-\frac{\sqrt{3}}{4} \approx -0.433$
^{87}Rb	2,2	2,1	$\frac{1}{4} \approx 0.250$
^{87}Rb	2,1	2,0	$\frac{\sqrt{6}}{8} \approx 0.306$
... and symmetrically for $-m_F \rightarrow -m_F - 1$			

Table 2.1: Selected transition amplitudes for ^{40}K and ^{87}Rb, expressed as multiples of $\mu_B B_{osc}$

2.5 Transition Probabilities and Field Amplitudes

As the atoms orbit in the trap, they pass through the region in which the energy level separation is resonant with the oscillating magnetic field, effectively sweeping through the resonance. The probability of the atom changing levels in one such sweep is [15]

$$P = 1 - \exp\left[\frac{-2\pi|\widehat{V}_{ij}|^2}{\hbar\Delta\dot{U}}\right] \tag{2.46}$$

where $|\widehat{V}_{ij}|$ is the relevant matrix element for the transition and $\Delta\dot{U}$ is the rate of the sweep, i.e. the rate of change of the energy difference between the two levels. In order to have an appreciable likelihood of successfully transferring the atoms in a single sweep, the perturbation must be strong enough that the argument of the exponential is of order unity. Now a typical $\Delta\dot{U}$ can be estimated from the thermal velocity of the atom and the trap gradient as

follows

$$\Delta\dot{U} = \frac{\partial \Delta U}{\partial B_{static}} |\nabla B_{static}| \, v_T \tag{2.47}$$

$$= (g'_F m'_F - g_F m_F)\mu_B \left(\frac{\mu_0 I}{2\pi r^2}\right) \sqrt{\frac{2k_B T}{m}} \tag{2.48}$$

For the worst-case $\left|F = \frac{9}{2}, m_F = \frac{9}{2}\right\rangle$ to $\left|F = \frac{7}{2}, m_F = \frac{7}{2}\right\rangle$ transition in ^{40}K[7], assuming a trap wire current of 3.5 A, 100 μm distance from wire to trap, 1 mK temperature[8] and 66×10^{-27} kg for the mass of ^{40}K gives a typical value of

$$\Delta\dot{U} \approx 7.5 \times 10^{-22} \text{ J/s} \tag{2.49}$$

$$\approx \hbar \times 2\pi \times 1.1 \text{ THz/s} \tag{2.50}$$

We therefore require a coupling amplitude of

$$|\widehat{V}_{ij}| \approx 1.1 \times 10^{-28} \text{ J} \tag{2.51}$$

$$\approx \hbar \times 2\pi \times 170 \text{ kHz} \tag{2.52}$$

The corresponding field amplitude is

$$B_{osc} \approx \frac{|\widehat{V}_{ij}|}{0.471\mu_B} \approx 26 \text{ μT} \tag{2.53}$$

This sets the order of magnitude of the field strength requirements[9]. Note that the evaporative cooling process saturates at a somewhat lower field strength, determined by the trap confinement and the rate of elastic and inelastic collisions among atoms in the cloud[16]. If the objectives of the system are restricted to evaporative cooling, then the magnetic field amplitude requirements derived above are over-stringent and may be relaxed substantially.

[7] Although some of the other transitions have less favourable matrix elements (see Table 2.1), the large $(g'_F m'_F - g_F m_F)$ factor makes the sweep particularly fast for this transition, and this effect dominates.

[8] The hottest atoms the system will be called upon to deal with.

[9] Strictly speaking, this value only applies for the ^{40}K microwave system that must drive the transition in question. However, similar calculations give 26 μT for the radio-frequency system and 21 μT for the ^{87}Rb microwave system, which are of the same order.

Chapter 3

Design and Implementation

Having described theoretically the objectives and performance requirements, we now turn to the practical design decisions that were made to achieve them. The project as a whole may be divided into three major systems: one for radio-frequency excitations corresponding to m_F-only transitions, operating between $2\pi \times 500$ kHz and $2\pi \times 30$ MHz with a precision of $2\pi \times 3$ kHz; one for microwave excitations across the hyperfine splitting in ^{40}K, operating between $2\pi \times 1.186$ GHz and $2\pi \times 1.386$ GHz again with a precision of $2\pi \times 3$ kHz; and one for microwave excitations across the hyperfine splitting in ^{87}Rb, operating between $2\pi \times 6.751$ GHz and $2\pi \times 6.919$ GHz with a precision of $2\pi \times 7$ kHz (c.f. Section 2.3). For each of these, a suitable high-frequency signal must be generated, amplified to useful power levels, and transmitted to the atoms by some form of antenna. Because of the limited lifetime of atoms in the trap, each system must be able to sweep through its full frequency range in about one second.

For the radio-frequency system, the signal generation and amplification circuitry had already been designed and implemented[17]. The remaining tasks were the design and construction of a suitable antenna. Work on the microwave systems started from a clean slate, and progressed as far as the implementation of a signal generation system for ^{40}K.

For each subsystem designed as part of the project, namely the radio-frequency antenna and ^{40}K signal generator, a brief summary of the practical requirements and constraints will be presented, followed by a description of the final design. For subsystems that did not reach final design, performance criteria, proposed technology and recommendations are reported in hopes that they may assist future work on this or similar projects.

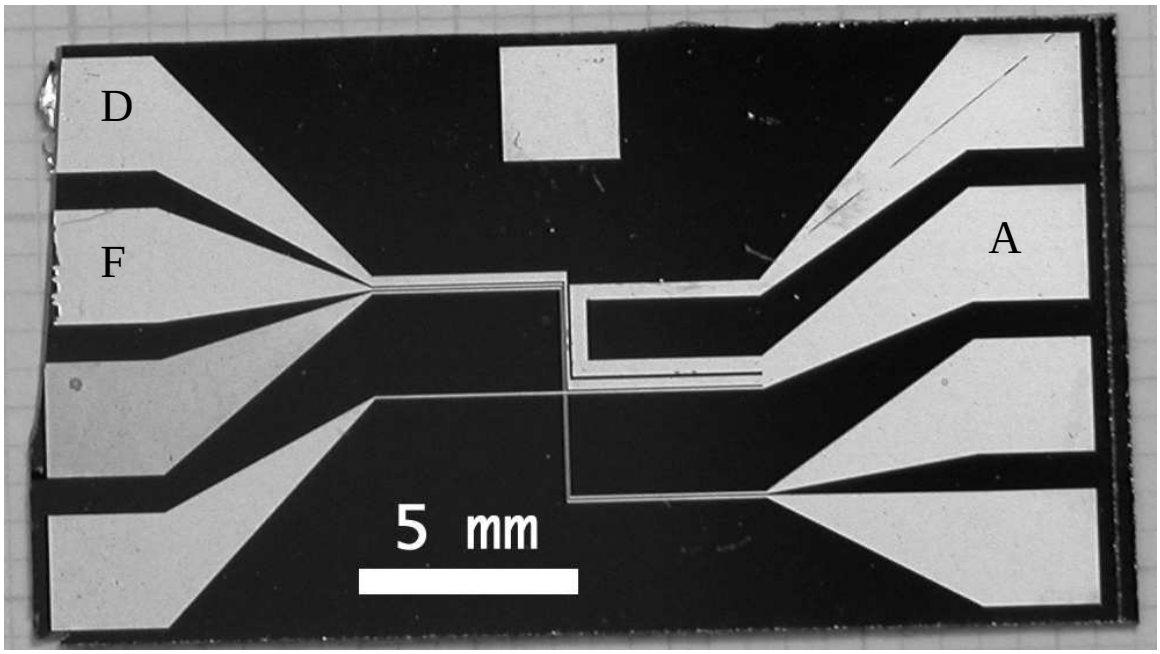

Figure 3.1: Layout of wires on the chip

Line A–D is used for magnetic trapping, line A–F is used as the antenna. The two are in electrical contact via pad A.

3.1 Radio-Frequency Antenna and Coupler Circuit

The practical constraints on this design are: a maximum power of 0.9 W, since that is the most the pre-existing amplification circuit can provide; no obstruction of the various laser beams used for cooling and imaging of the atoms; no modifications to the contents of the vacuum chamber housing the experiment, which cannot be opened without significantly delaying the work of other users of the apparatus; and minimal power reflected back along the transmission line, to avoid damaging the amplifier.

The design that was adopted sends the radio-frequency signal to a pre-existing wire on the micro-fabricated chip trap (see Figure 3.1). This neatly addresses the power requirements. The wire being situated only 100 μm from the trapped atoms, the field amplitude is[1]

$$B = \frac{\mu_0 I}{2\pi \times 100\ \mu\text{m}} = (2\ \text{mT/A}) \times I \tag{3.1}$$

The 0.9 W AC output of the final amplifier, attenuated by 3 dB (see the end of this section for an explanation), travelling on a 50 Ω transmission line generates a peak current amplitude of 135 mA, so the atoms can be subjected to fields of ∼ 270 μT, an order of

[1]Since the distances involved are much shorter than the free-space wavelength at 30MHz, we can safely use DC field analysis.

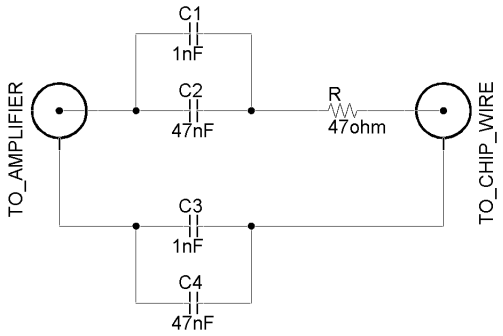

Figure 3.2: Radio-frequency coupler circuit

This provides DC decoupling of the antenna from the amplifier. The capacitors pass the radio-frequency signal but block any static voltages on either line. The resistor provides a limited form of impedance matching.

magnitude better than the estimated requirement. The actual performance will vary depending on the presence of standing waves in the transmission line. If the chip wire acts as a short-circuit line termination, leading to a current anti-node, performance might be improved by a factor of two.

Since it does not involve the construction and installation of a dedicated antenna, this system trivially avoids the problem of positioning the antenna outside the laser beam paths and was set up without interrupting normal use of the experimental apparatus.

However, since the various wires on the chip are all interconnected, and since large DC currents flow through some of them in order to set up the static fields necessary for magnetic trapping, the use of a chip wire as an antenna introduces an additional requirement. The radio-frequency circuitry must, at DC, be completely disconnected from the chip wire, both to avoid disrupting the normal operation of the magnetic trap and to protect the amplifier from externally applied voltages. This requirement is addressed by a "coupler circuit" (see Figure 3.2), situated on the transmission line about one metre before the chip, which acts as a high-frequency-only connection between the chip wire used as an antenna and the output of the signal amplifier.

Each conductor on the transmission line is interrupted by a pair of capacitors. The larger of the two is chosen to pass a $2\pi \times 500$ kHz signal, using the guideline that the reactance and resistance should be equal at one-half the desired minimum operating frequency[18]. The smaller bypass capacitors correct for parasitic inductance in the large capacitor at high frequencies.

The coupler circuit also includes a 47 Ω resistor which serves to match the 1 Ω chip wire to the 50 Ω transmission cable. The matching is only approximate since the section

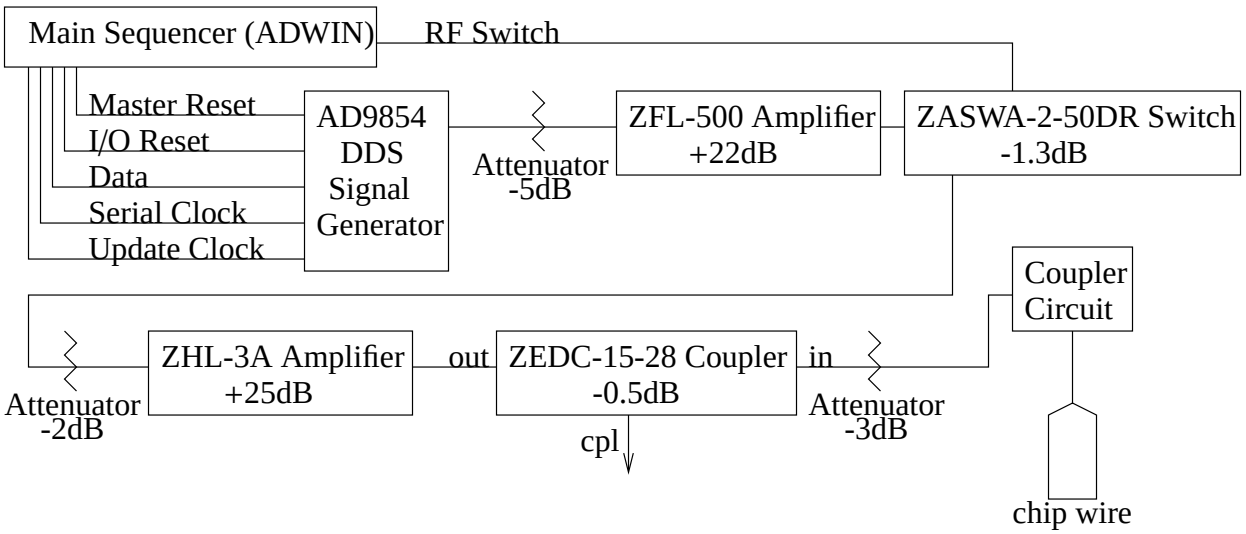

Figure 3.3: Schematic of the complete signal path for the radio-frequency system

The ADWIN sequencer is the main controller for the experiment as a whole, and sends digital commands to the DDS to control generation of the radio-frequency signals, synchronised with the remainder of the apparatus. The separately controlled switch (top right) serves to interrupt any residual signal from the DDS for those parts of the experimental cycle where no radiation is desired. The attenuators before each amplifier serve to protect them from over-powered input signals and from possible reflections between components. The final-stage ZHL-3A amplifier's maximum output power is 29.5 dBm $\approx$ 900 mW. The ZEDC directional coupler serves to monitor reflected power from the load.

of transmission line inside the vacuum chamber has significant parasitic reactances and because a partial standing wave may arise between the chip and the coupler circuit, altering the load impedance seen by the latter in a frequency-dependent manner. It is difficult to devise a more exact matching circuit because of the large bandwidth it must cover. With the current system, measurements using a directional coupler show that less than $1/4$ the power is reflected to the amplifier in the worst case. Unfortunately, the maximum allowable reflected power for the final-stage amplifier is not documented. However, its output VSWR in the frequency range of interest is specified to be in the range 1.65–1.7, which is indicative of the level of acceptable impedance mismatch[2]. As a safety precaution, a 3 dB attenuator has been placed after the final amplifier. It reduces the output current amplitude by a factor of $1/\sqrt{2}$ but reduces the power reflected to the amplifier by a factor of $1/4$, i.e. $1/2$ on each of the outbound and return journeys.

[2]The VSWR (Voltage Standing Wave Ratio) is the ratio of the sum to the difference of the forward and reverse wave amplitudes or, equivalently, of the node to antinode amplitude in the overall standing wave. A VSWR of 1.7 corresponds to 7% reflected power.

3.2 Microwave Signal Generation for ^{40}K

The generation of suitable microwave signals for driving hyperfine transitions poses additional challenges because the requirements exceed the capabilities of commercially available signal generators. Although some high-precision signal generators such as the Agilent 8257D cover the frequency range in question, they are designed for operation at a stable frequency, with frequency switching times on the order of tens of milliseconds. Since a 1 s ramp used for evaporative cooling might involve around 700 frequency changes (assuming constant-ratio steps and an end resolution of $2\pi \times 3$ kHz) these generators are about 10 times too slow to achieve the required sweep rate. Direct digital synthesis systems have the requisite sweep rates and accuracy (and are comparatively inexpensive), but the fastest ones currently available have output rates of 10^9 sample/s. Since the output frequency is limited by the Nyquist theorem, the maximum useful output frequency is around $2\pi \times 400$ MHz.

The solution currently being implemented uses an Analog Devices AD9858 DDS synthesiser operating in the range of $2\pi \times (295 - 347)$ MHz and two doublers to quadruple its output frequency into the required range. The advantages of this scheme, compared to some of those to be examined in Section 3.3, are threefold: conceptual simplicity, easy assembly from coaxial-connector components, and a small number of easily controlled sources of frequency instability.

This last factor is crucial: to achieve $2\pi \times 3$ kHz frequency precision on a $2\pi \times 1.3$ GHz signal requires stability at the 2 ppm level. Having many or large sources of frequency jitter in the signal path is therefore unacceptable. Fortunately, the output frequency of a harmonic multiplier is directly proportional to that of the input signal coming from the DDS. The DDS, in turn, has a stability that is practically limited only by its clock. In order to achieve the desired performance from this component, a high-precision oven-controlled crystal oscillator at $2\pi \times 60$ MHz is used as the master reference in a phase-locked loop, to which a narrow-band voltage-controlled oscillator operating at $2\pi \times 960$ MHz is slaved. The output of this oscillator serves as a clock signal for the DDS. Since this portion of the system operates at fixed frequency, it need not have a rapid response time, and can be made very stable using a narrow-band low-pass filter in the phase-locked loop.

Having established an accurate sample clock reference for the DDS, the only remaining sources of noise in the output signal are harmonics generated by the digital output waveform and the multipliers. Fortunately, these tend to be suppressed by the non-linear behaviour of the multipliers and, being widely separated in frequency, are easy to filter. The largest spur in the unfiltered output of the multiplier chain is expected to be at one-half the main output frequency, around $2\pi \times 640$ MHz, and is smaller than the main peak

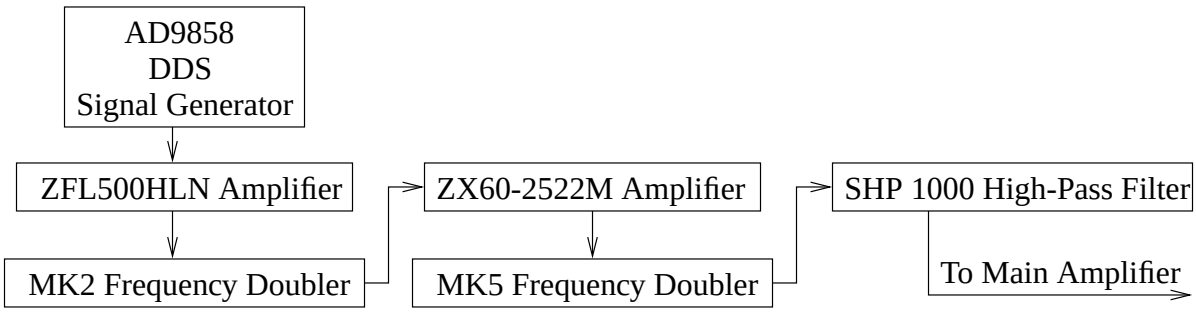

Figure 3.4: Schematic of the signal generation portion of the ^{40}K microwave generator

The intermediate amplifiers compensate for power loss in the multipliers. Within each column the carrier frequency is constant, changes of column to the right indicate doubling of the carrier frequency.

by 13 dB or more; a high-pass filter with a cut-off frequency of $2\pi \times 900$ MHz suppresses it by an additional 20 dB. The multipliers should suppress other spurs by at least 40 dB. A low-pass filter could easily be added if higher-frequency harmonics are found to be a problem.

A few simple modifications to the AD9858 board are required: replacing the pre-existing voltage-controlled oscillator, which operates at the wrong frequency for our purposes, and adding extra capacitance to the phase-locked loop. The remainder of the implementation effort for this section is devoted to correctly mounting, cooling, interconnecting, and delivering low-noise power to the AD9858 board, the reference crystal, and the multiplier chain, as well as developing appropriate control software to drive the DDS.

3.3 Comments on Microwave Signal Generation for ^{87}Rb

As with the ^{40}K system, the fundamental challenge is to take the fast-sweeping but low-frequency DDS output and generate from it a high-frequency signal while preserving a frequency stability of $2\pi \times 7$ kHz (absolute) or 1 ppm (relative). There are two basic approaches to raising the frequency of the signal: multiplication and addition.

In the multiplicative case, the overall frequency stability can be no better than the relative stability of the DDS clock, which must therefore satisfy the 1 ppm constraint mentioned above. Also, assuming a maximum DDS output frequency of $2\pi \times 400$ MHz, the frequency must be multiplied by at least 17 (or more likely by 32, the next power of 2) to reach the required output frequency band. This can be accomplished using either harmonic multipliers or a phase-locked loop. Using off-the-shelf doublers, as with the ^{40}K system, would require 5 stages (with intermediate amplifiers), the last few of which would

require special assembly as coaxial-connector mixers are rare above $2\pi \times 2$ GHz. It might be possible instead to use a bandpass filter to select the appropriate harmonic of the DDS output (possibly after passing the output through a fast switch to convert the signal to a square wave with larger harmonic components) thus reducing the system to a single stage. A phase-locked loop could be used instead of multipliers, provided that it did not introduce excessive frequency jitter. Since the shortest required response time of the loop is of the order of tens of microseconds (corresponding to a sweep through $2\pi \times 100$ MHz in $2\pi \times 7$ kHz steps in 1 second) and the loop output period is of the order of 0.1 ns, this is feasible in principle.

Instead of scaling up the DDS output frequency range by a constant factor, the additive approach would translate it by a constant offset, mixing it with a stable high-frequency source. One advantage of this method is that it might allow the use of a DDS with a lower output frequency (since the frequency offset can be varied independently) as long as it had the requisite $2\pi \times 168$ MHz bandwidth. Such a synthesiser would be less expensive and easier to clock. The frequency stability of this system would be as good as the sum of the absolute frequency jitters on the DDS clock signal and the high-frequency reference signal. Although this would require finding an extremely precise high-frequency reference, it would place a much less stringent requirement on the low-frequency portion of the system. Some additional points should be considered for the design of such a system. The mixing should most likely take place before the final signal amplification, both to minimise power loss in the final signal and to take advantage of less expensive low-power mixers. The mixer should be chosen to be of the common "single side-band" type, to avoid saturating amplifiers with the undesirable fixed-frequency carrier signal. Care must also be taken to select an up-mixer and not a down-mixer. The requirement here is that the mixer's specified "RF" frequency range include the operating frequencies of the DDS, that its "IF" range include the requisite output band, and that the "LO" frequency correspond to the stable high-frequency reference. Preliminary investigations have not revealed any commercially available components that meet these requirements.

3.4 Comments on Microwave Antennae

The use of chip wires for broadcasting microwave radiation is certainly an option and, in theory, could work just as well as for the radio-frequency case. However, the skin depth is much reduced at high frequencies; for the gold chip wire, the skin depth is 14 μm at $2\pi \times 30$ MHz but only 2.2 μm at $2\pi \times 1.28$ GHz and 0.95 μm at $2\pi \times 6.8$ GHz. Combined with the unknown and difficult-to-measure reactive behaviour of the wires in the chip's

support structure, this may make it difficult to drive sufficient current through the chip wire to achieve adequate performance. However, it is by far the simplest solution, and should be investigated more thoroughly before turning to the rather daunting alternatives to be described below.

The use of a focused or collimated beam of far-field microwave radiation from outside the vacuum cell would require a great deal of power. For the ^{40}K system, with a free-space wavelength of 0.23 m, the necessary time-averaged far-field power flux to sustain the required magnetic field amplitude is

$$\frac{\eta}{2}\left(\frac{B}{\mu_0}\right)^2 \approx 80 \text{ kW/m}^2 \tag{3.2}$$

Assuming, optimistically, that the focusing elements can be arranged to have a numerical aperture of 0.5 — i.e. a vertex angle of $\pi/6$ — the area of the beam waist would be at least

$$\pi r^2 \approx \pi\left(\frac{\lambda}{\pi\theta}\right)^2 \approx \frac{36\lambda^2}{\pi^3} \approx 6.3\times10^{-2} \text{ m}^2 \tag{3.3}$$

where we have assumed a Fourier-limited Gaussian profile[19, p488]. The estimated power requirement is therefore around 5 kW. A similar calculation for the ^{87}Rb system gives a requirement of 120 W because of the shorter wavelength and slightly weaker field. Since the power requirement is proportional to the square of the field strength, any reduction in the magnetic field requirement, for instance by restricting the function of these systems to evaporative cooling, will dramatically affect these estimates. On the other hand, real-world beam focusing is unlikely to be as good as has been assumed here, in particular given the perturbing effects of the large conducting chip support structure. It would seem, then, that some form of near-field enhancement is needed.

For the ^{40}K system, where the wavelength is greater than the vacuum cell's transverse dimension, it may be possible to achieve near-field effects from outside the waveguide. For the ^{87}Rb system, where the wavelength is only 4.4 cm, modifications inside the vacuum chamber are likely to be necessary. This may involve placing the antenna inside the chamber very near the trap, using a waveguide (a simple dielectric bar might suffice) to channel power from a more conveniently positioned antenna to the trap, or installing a small dielectric sphere near the trap to act as a resonator[20].

Chapter 4

Conclusion

A suite of tools for transferring trapped ^{40}K and ^{87}Rb atoms between hyperfine and Zeeman sublevels using radio-frequency and microwave oscillating magnetic fields would be a valuable addition to the experimental capabilities of the Ultra-Cold Atoms Laboratory. It would allow the use of evaporative cooling techniques for bringing clouds of atoms to quantum degeneracy, offer the ability to perform energy spectroscopy of the cooled clouds, and provide the means to create coherent mixtures of atoms in different states with which to explore a rich area of quantum phenomena. Although not yet reached, the goal of constructing such a suite has been brought significantly closer. A theoretical treatment of the problem has been given, leading to estimated performance requirements and constraints. In particular, the frequency ranges of immediate interest and the necessary field amplitudes have been computed, and general formulae have been developed to facilitate analysis of similar problems in future. A radio-frequency system for driving Zeeman transitions, using a wire on the trapping chip itself as an antenna to transmit the radiation, has been completed and is currently being evaluated. A signal generator capable of supplying an accurate, rapidly swept signal in the frequency ranges of interest for transitions across the hyperfine split in ^{40}K has been designed and is presently being constructed. Finally, some suggestions have been made for the implementation of the antennae and signal generators that have yet to be built; suggestions which, it is hoped, will serve as a useful starting point for upcoming work to complete this project.

Bibliography

[1] M. H. Anderson, J. R. Ensher, M. R. Matthews, C. E. Wieman, and E. A. Cornell, "Observation of Bose-Einstein condensation in a dilute atomic vapor," *Science*, vol. 269, pp. 198–201, 1995.

[2] C. C. Bradley, C. A. Sackett, J. J. Tollett, and R. G. Hulet, "Evidence of Bose-Einstein condensation in an atomic gas with attractive interactions," *Phys. Rev. Lett.*, vol. 75, no. 9, pp. 1687–1690, 1995.

[3] K. B. Davis, M.-O. Mewes, M. R. Andrews, N. J. van Druten, D. S. Durfree, D. M. Kurn, and W. Ketterle, "Bose-Einstein condensation in a gas of sodium atoms," *Phys. Rev. Lett.*, vol. 75, no. 22, pp. 3969–3973, 1995.

[4] B. DeMarco and D. S. Jin, "Onset of Fermi degeneracy in a trapped atomic gas," *Science*, vol. 285, no. 5434, pp. 1703–1706, 1999.

[5] A. G. Truscott, K. E. Strecker, W. I. McAlexander, G. B. Partridge, and R. G. Hulet, "Observation of Fermi pressure in a gas of trapped atoms," *Science*, vol. 291, no. 5513, pp. 2570–2572, 2001.

[6] F. Schreck, L. Khaykovich, K. L. Corwin, G. Ferrari, T. Bourdel, J. Cubizolles, and C. Salomon, "Quasipure Bose-Einstein condensate immersed in a Fermi sea," *Phys. Rev. Lett.*, vol. 87, no. 8, p. 080403, 2001.

[7] S. Aubin, M. Extavour, S. Myrskog, L. LeBlanc, J. Estève, S. Singh, P. Scrutton, D. McKay, R. McKenzie, I. Leroux, A. Stummer, and J. H. Thywissen, "Trapping fermionic ^{40}K and bosonic ^{87}Rb on a chip," *J. Low Temp. Phys.*, February 2005. Submitted.

[8] W. Ketterle, D. S. Durfee, and D. M. Stamper-Kurn, "Making, probing and understanding Bose-Einstein condensates," in *Bose-Einstein Condensation in Atomic Gases* (M. Inguscio, S. Stringari, and C. E. Wieman, eds.), vol. 140, International School of Physics "Enrico Fermi", Italian Physical Society, 1999. arXiv:cond-mat/9904034.

[9] A. Browaeys, A. Robert, O. Sirjean, J. Poupard, S. Nowak, D. Boiron, C. I. Westbrook, and A. Aspect, "Thermalization of magnetically trapped metastable helium," *Phys. Rev. A*, vol. 64, no. 3, p. 034703, 2001.

[10] R. Shankar, *Principles of Quantum Mechanics*. New York: Kluwer Academic/Plenum Publishers, second ed., 1994.

[11] D. R. Lide, ed., *CRC Handbook of Chemistry and Physics*. CRC Press, 85th ed., 2004. http://www.hbcpnetbase.com/.

[12] C. Cohen-Tannoudji, B. Diu, and F. Laloë, *Quantum Mechanics*, vol. 2. Toronto: John Wiley and Sons, 1977.

[13] J. H. Thywissen, 2005. Private Communication.

[14] C. Cohen-Tannoudji, "Cours de Claude Cohen-Tannoudji au Collège de France, année scolaire 1976-77." `http://www.lkb.ens.fr/cours/college-de-france/1976-77/1976-77.htm`, 1976.

[15] C. Zener, "Non-adiabatic crossing of energy levels," *Proceedings of the Royal Society of London. Series A, Containing Papers of a Mathematical and Physical Character*, vol. 137, no. 833, pp. 696–702, 1932.

[16] W. Ketterle and N. J. van Druten, *Evaporative Cooling of Trapped Atoms*, vol. 37, pp. 181–236. San Diego: Academic Press, 1996.

[17] D. McKay, "Summer 2004 report." `http://www.physics.utoronto.ca/~jhtgroup/reprints/McKay04.pdf`, October 2004.

[18] A. Stummer, 2004. Private Communication.

[19] P. W. Milonni and J. H. Eberly, *Lasers*. Toronto: John Wiley & Sons, 1988.

[20] J. B. Pendry, November 2004. Private Communication.

Appendix A

Power Supply for the ^{40}K Microwave System

Figure A.1 shows the power supply and external connections for the ^{40}K microwave system's signal generator and associated components. It provides four separate outputs:

- An unprocessed 9V line to drive the cooling fan.
- A regulated 5 V supply for the frequency dividers and charge pump in the phase-locked loop.
- A regulated 3.3 V supply for the DDS chip itself.
- A second regulated 5 V supply for the clock oscillators, the master oven-controlled crystal (OCXO) and the slaved voltage-controlled oscillator (VCO). A separate supply with a larger filtering capacitor is provided to ensure the stability of these two oscillators, which determines the frequency precision of the signal generator as a whole.

To avoid overheating, the regulators are clamped, via electrically-insulating but thermally-conducting pads, to a steel casing which acts as a large heat sink. Also, the unnecessarily large voltage drop from the 9 V supply to the 5 V regulator output is reduced using pairs of forward-biased diodes, which are robust enough to dissipate the excess power without being damaged. A commercial transformer-rectifier connected to the mains provides the 9 V DC supply.

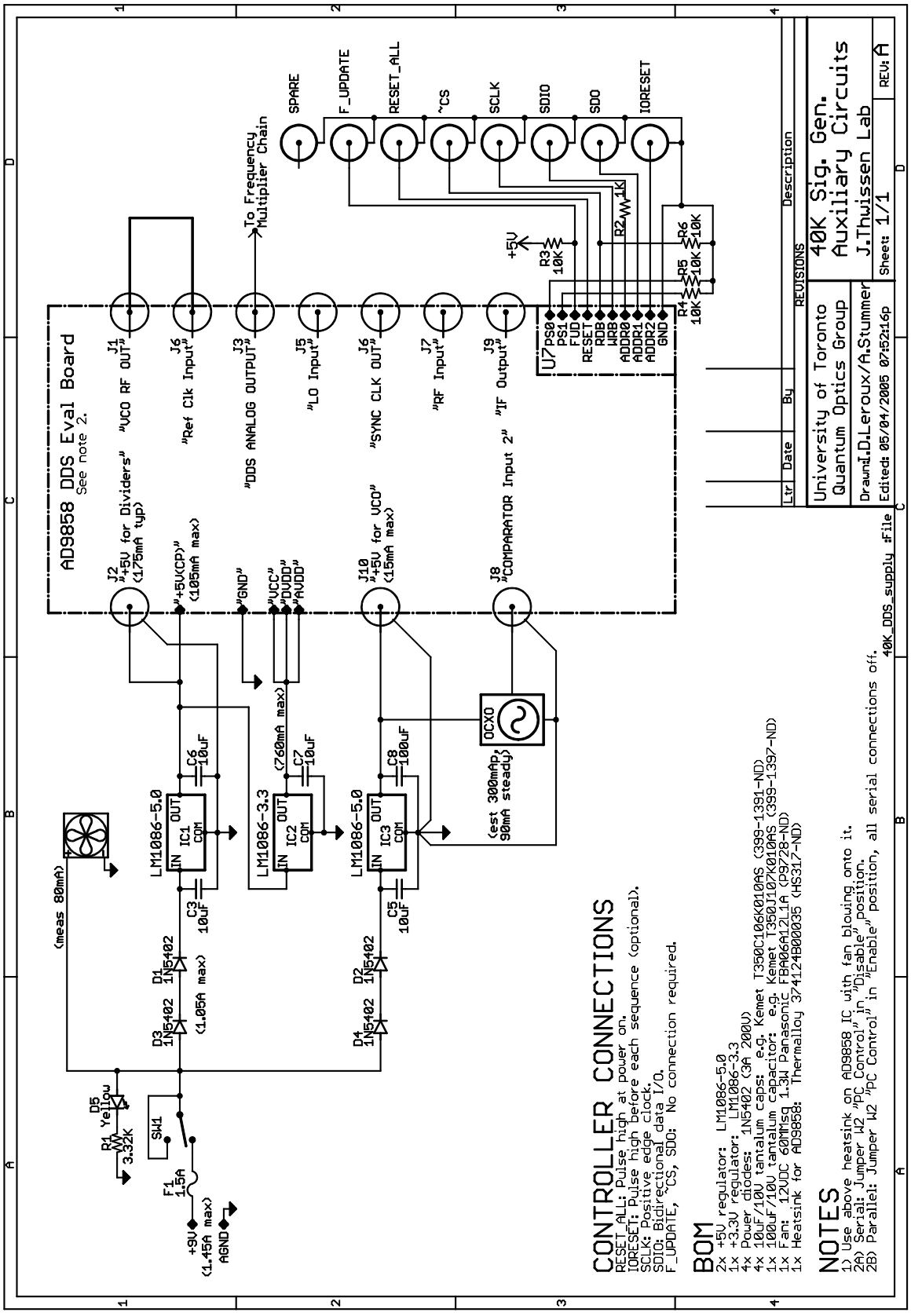

Figure A.1: Schematic of power supply circuitry for the signal generation section of the ^{40}K microwave system